JOC The Journal of Organic Chemistry

Article

pubs.acs.org/joc

Mechanistic Insights into Bicyclic Guanidine-Catalyzed Reactions from Microscopic and Macroscopic Perspectives

Hansong Xue,[†] Danfeng Jiang,[†] Huan Jiang,[†] Choon Wee Kee,[†] Hajime Hirao,[†] Takahiro Nishimura,[§] Ming Wah Wong,*[,‡] and Choon-Hong Tan*[,†]

[†]Department of Chemistry and Biological Chemistry, Nanyang Technological University, 21 Nanyang Link, Singapore 637371

[‡]Department of Chemistry, National University of Singapore, 3 Science Drive 3, Singapore 117543

[§]Department of Chemistry, Kyoto University, Sakyo-ku, Kyoto 6068502, Japan

Supporting Information

ABSTRACT: Chiral bicyclic guanidine can act as an efficient chiral Brønsted base catalyst in enantioselective reactions, delivering good yields with high enantioselectivities. There is interest in understanding the detailed mechanisms of these guanidine-catalyzed reactions. Herein, we performed a detailed kinetic study of three different types of chiral bicyclic guanidine-catalyzed reactions, determining the bifunctionality of our guanidine catalyst. Although these three reactions share a similar catalytic cycle, their intrinsic kinetic behaviors are significantly different from each other because of the difference in the rate-determining step. The calculated theoretical rate expression for each reaction, as a result of the mechanism elucidated with density functional theory calculations, agrees well with the respective experimentally observed rate equation.

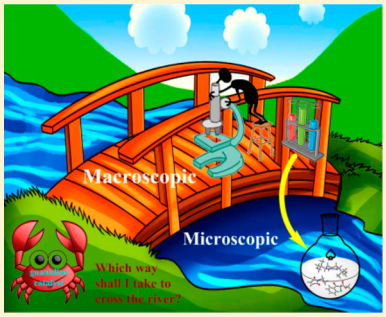

INTRODUCTION

Guanidine is well-known for its efficient catalytic abilities as a nucleophilic or Brønsted base.[1] Recently, it has attracted a great deal of attention because of its prominent role in organocatalysis.[2] When guanidine acts as a Brønsted base catalyst, the guanidinium cation formed from deprotonation of the substrate participates in the reaction by utilizing hydrogen bonding[3] and ion-pair interaction. The guanidinium ion can activate a nucleophile in a monofunctional mode or both an electrophile and a nucleophile in a bifunctional mode (Scheme 1).[1]

Scheme 1. Ion-Pair Interaction and Hydrogen Bonding of the Guanidinium Cation with Substrates

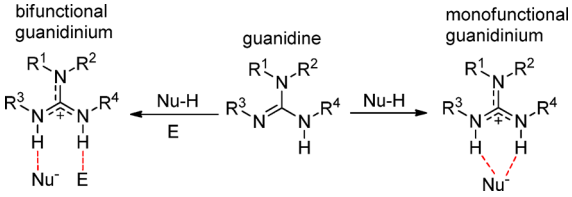

In the monofunctional activation mode, it was proposed that the guanidinium ion formed either a single hydrogen bond or dual hydrogen bonds to a single substrate (Scheme 1). Furthermore, it was proposed that aza-Michael reactions,[4] Michael reaction of glycinate,[5] Henry reactions,[6] epoxidation reactions,[7] and Claisen rearrangement reactions may go through a dual hydrogen bonding to a single substrate.[8] In the Claisen rearrangement reactions catalyzed by a guanidinium salt, Uyeda and Jacobsen have confirmed such a dual hydrogen bonding mode with X-ray crystallographic analysis and DFT calculation.[8] On the other hand, for hydroxyguanidine-catalyzed Michael reactions,[9] guanidine-catalyzed intramolecular Michael reactions,[10] bis-guanidine-catalyzed IEDDA,[11] and guanidine-catalyzed desymmetrization of meso *N*-acylaziridines,[12] the authors proposed that the catalyst has only a single hydrogen bond to a single substrate.

In the bifunctional activation mode, the guanidinium intermediate formed hydrogen bonds with the substrate (Nu^-) as well as the incoming electrophile (E) to generate a pre-transition-state ternary intermolecular complex (Scheme 1).[1] Corey, Ma, Feng, and Tereda proposed this bifunctionality in the enantioselective Strecker reaction,[13] Michael reaction of anthrone,[14] Michael reaction of β-ketoesters with nitroolefins,[15] and vinylogous aldol reaction,[16] respectively. We also provided preliminary support for this postulate by analyzing the X-ray structure of TBD·HCl·H_2O.[17]

DFT studies of the Michael reaction of fluorocarbon nucleophiles[18] and biomimetic decarboxylation Mannich and decarboxylative amination reactions revealed this bifunctionality of the guanidinium catalyst.[19] In a DFT study of the guanidine-catalyzed phospha-Michael reaction of β-nitrostyrene, this bifunctional activation role of guanidine was clearly revealed in all three steps of the proposed catalytic cycle, namely, tautomerization of diphenylphosphine oxide, followed by carbon−phosphorus bond formation and last concerted hydrogen transfer.[20] In addition, we found an unconventional bifunctional mode of Lewis and Brønsted acid activations in a

Received: March 31, 2015
Published: May 14, 2015

DOI: 10.1021/acs.joc.5b00709
J. Org. Chem. 2015, 80, 5745−5752

DFT study of the guanidine-catalyzed thio-Michael reaction.[21] As indicated in Scheme 2, there are two possible bifunctional

Scheme 2. Two Possible Bifunctional Modes of Activation of Bicyclic Guanidinium Ion

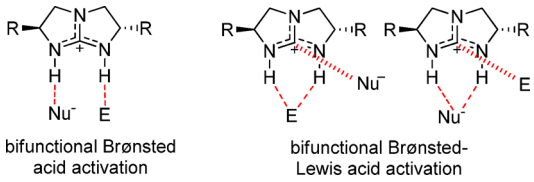

activation modes of the bicyclic guanidinium catalyst, normal bifunctional Brønsted acid activation mode and unconventional bifunctional mode of Lewis and Brønsted acid activation. Bifunctional Brønsted–Lewis acid activation provides an alternate reaction pathway of the guanidine-catalyzed thio-Michael reaction, and this pathway strongly influences the final stereochemical outcome of the addition.

Reaction progress kinetic analysis (RPKA)[22] is a powerful methodology developed by Blackmond to study kinetic and mechanistic properties of a complicated catalytic system under synthetically relevant conditions, rather than using the highly distorted concentration ratios as required in classic kinetic analysis. The kinetic behavior can be rapidly and quantitatively investigated from significantly fewer experiments. To gain a better understanding of the intrinsic kinetic behavior of [5,5] bicyclic guanidine catalyst **1** (Scheme 3) and illuminate its role

Scheme 3. Proposed Mechanism of the Guanidine-Catalyzed Phospha-Michael Reaction between Diphenylphosphine Oxide 2 and β-Nitrostyrene 3

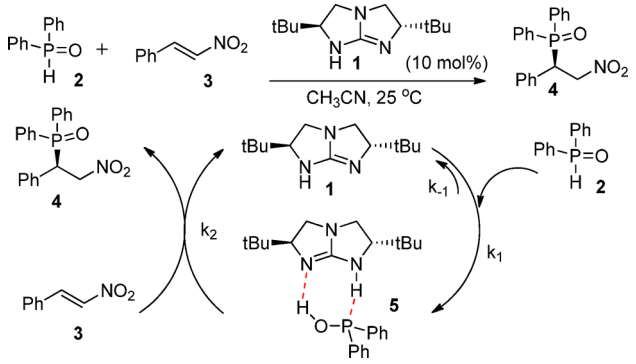

in the catalytic cycle, herein we report a detailed kinetic study of three guanidine-catalyzed reactions: (a) phospha-Michael reaction of β-nitrostyrene,[23] (b) addition reaction of fluorocarbon nucleophiles,[18] and (c) isomerization reaction of alk-3-ynoate.[24] All three reactions were continuously monitored in a reaction calorimeter (Ominical SuperCRC) with WinCRC software and the RPKA method of "excess" relationship,[22] and a graphical rate equation was adopted to investigate the kinetic behavior.

RESULTS AND DISCUSSION

Phospha-Michael Reaction of β-Nitrostyrene. The catalytic cycle for the phospha-Michael reaction between diphenylphosphine oxide **2** and β-nitrostyrene **3** is outlined in Scheme 3. When the rate versus the concentration of diphenyl-phosphine oxide ([**2**]) was plotted for two reactions under the same "excess" condition, the overlay of curves a and b in Figure 1 suggests no catalyst deactivation throughout the

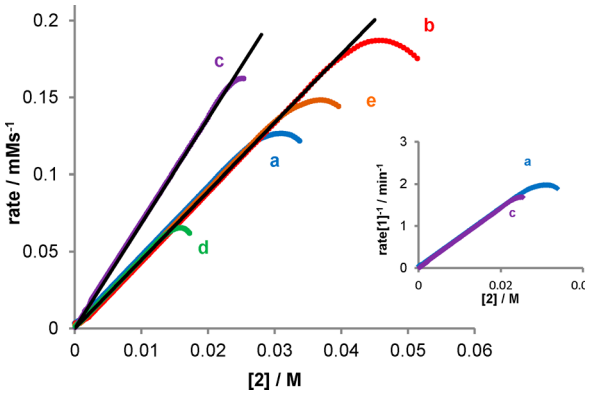

Figure 1. Graphical rate equations for the guanidine-catalyzed phospha-Michael reaction between diphenylphosphine oxide and β-nitrostyrene (Scheme 3). The inset shows the rate vs [**2**] and rate/[**1**] vs [**2**]. The solid black lines represent the kinetic model given in eq 1. Reaction conditions: (a) $[\mathbf{2}]_0$ = 38.4 mM, $[\mathbf{3}]_0$ = 76.9 mM, $[\mathbf{1}]_{total}$ = 3.84 mM; (b) $[\mathbf{2}]_0$ = 57.7 mM, $[\mathbf{3}]_0$ = 96.2 mM, $[\mathbf{1}]_{total}$ = 3.84 mM; (c) $[\mathbf{2}]_0$ = 30.8 mM, $[\mathbf{3}]_0$ = 53.8 mM, $[\mathbf{1}]_{total}$ = 5.76 mM; (d) $[\mathbf{2}]_0$ = 19.2 mM, $[\mathbf{3}]_0$ = 42.3 mM, $[\mathbf{1}]_{total}$ = 3.84 mM; (e) $[\mathbf{2}]_0$ = 46.1 mM, $[\mathbf{3}]_0$ = 115 mM, $[\mathbf{1}]_{total}$ = 3.84 mM.

reaction. In addition, the overlay of curves a, d, and e from reactions employing different "excess" conditions allows us to conclude zero-order kinetics in the concentration of β-nitrostyrene ([**3**]). First-order kinetics in the concentration of diphenylphosphine oxide ([**2**]) is confirmed from the straight line plot. The rate divided by the concentration of guanidine ([**1**]) is plotted versus [**2**] in the inset of Figure 1 to show that the reaction is indeed first-order with respect to guanidine catalyst **1**.

From the relationship obtained from Figure 1, the overall rate expression is determined to be eq 1, where k_1 is determined to be 1.16 M^{-1} s^{-1} (standard deviation of 1.12%; R^2 = 0.998; SSE = 0.0002).

$$\text{rate} = k_1[\mathbf{2}][\mathbf{1}]_{total} \quad (1)$$

There are three steps in the catalytic cycle. Diphenylphosphine oxide **2** is deprotonated by guanidine **1** to form intermediate complex **5** in the first step, followed by the addition of **5** to β-nitrostyrene to form the final product **4**, and the catalyst goes back to its original form, **1**. The rate equation (eq 1) reveals that the first deprotonation step is slow, which is the rate-determining step; the second step is relatively fast where the formation of the intermediate **5** is rate-limiting and the unbound guanidine catalyst **1** is in the "resting state". This corresponds well to our earlier computational results where the first step is predicted to have an activation barrier ($\Delta G^{\ddagger}$ = 56.7 kJ mol^{-1}) significantly higher than that of the second step ($\Delta G^{\ddagger}$ = 46.0 kJ mol^{-1}).[20] There is a possibility that diphenylphosphine oxide **2** may undergo uncatalyzed tautomerization to form phosphinic acid. However, this pathway is less likely because of its higher calculated activation barrier.[20]

Addition Reaction of Fluorocarbon Nucleophiles. Similar to the phospha-Michael reaction, the catalytic cycle for guanidine-catalyzed addition of a fluorocarbon nucleophile between α-fluoro-β-ketoester **6** and *N*-ethylmaleimide **7** consists of initially the transfer of a proton from the α-fluoro-

DOI: 10.1021/acs.joc.5b00709
J. Org. Chem. 2015, 80, 5745–5752

β-ketoester **6** to guanidine catalyst **1** and a hydrogen-bonded ternary complex formed of the guanidinium cation, the ketoester anion, and *N*-ethylmaleimide in the second step (Scheme 4). On the basis of the kinetic model proposed by

Scheme 4. Proposed Mechanism of Guanidine-Catalyzed Addition of α-Fluoro-β-ketoester 6 to *N*-Ethylmaleimide 7

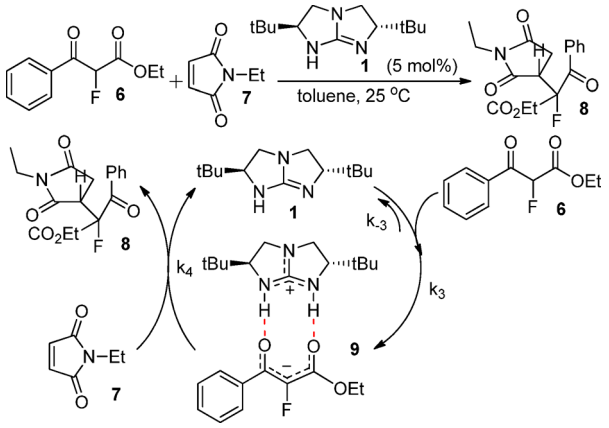

Blackmond[22a] and examination of the curves in panels 2iii and 2iv of Figure 2, we conclude that the reaction has first-order kinetics with respect to *N*-ethylmaleimide **7** but complex-order kinetics with respect to α-fluoro-β-ketoester **6**. Moreover, panels 2i and 2ii of Figure 2 reveal the catalyst concentration is stable and the reaction is first-order in guanidine concentration throughout the entire course of the reaction. The shape of the curves in panel 2iv of Figure 2 indicates a possibility of saturation kinetics behavior in the concentration of α-fluoro-β-ketoester ([**6**]) with the Michaelis–Menten equation[22a]

$$\frac{\text{rate}}{[\mathbf{7}]} = \frac{V_{\max}[\mathbf{6}]}{K_M + [\mathbf{6}]} \tag{2}$$

where $V_{\max} = k_4[\mathbf{1}]_{\text{total}}$ and $K_M = k_{-3}/k_3$.

The double-reciprocal plot of eq 2 gives the Lineweaver–Burk equation that linearly relates [**7**]/rate and 1/[**6**].

$$\frac{[\mathbf{7}]}{\text{rate}} = \frac{K_M}{V_{\max}}\frac{1}{[\mathbf{6}]} + \frac{1}{V_{\max}} \tag{3}$$

As shown in panel 2v of Figure 2, the linear relationship of the experimental data in the Lineweaver–Burk plot allows us to conclude the exisence of saturation kinetics in the concentration of α-fluoro-β-ketoester ([**6**]), with a calculated Michaelis constant of 0.0842 M (standard deviation of 1.26%) and a $V_{\max}$ of 0.00308 s^{-1} (standard deviation of 0.50%). Hence, this reaction exhibits overall first-order kinetics in the concentration of *N*-ethyl maleimide ([**7**]) and a saturation kinetics behavior in the concentration of α-fluoro-β-ketoester ([**6**]).

Formation of a binary ion-pair complex **9** is a key step in the catalytic cycle. This complex, **9**, is characterized by dual hydrogen bonds between the guanidinium NH protons and the oxygen atoms of the carbonyl groups in the enolate anion. This ion-pair complex can readily be formed by the transfer of a proton from the α-fluoro-β-ketoester to the guanidine catalyst via a weak guanidine–ketoester neutral complex. The calculated barrier ($\Delta G^{\ddagger}$) is small, 34.2 kJ mol^{-1}, for such a proton transfer process (Supporting Information). *N*-Ethylmaleimide can approach guanidinium–enolate ion-pair complex **9** to form the pre-TS ternary complex and corresponding C···C forming the TS in either a face-on (bifunctional Brønsted acid activation) or a side-on (bifunctional Brønsted–Lewis acid activation) manner.[18,25] Our current calculations, at the M06-2X/6-311+G** level together with the SMD solvation model (in toluene solvent), confirm the previous theoretical finding[18] that the side-on transition states are more stable than the corresponding face-on transition states. In excellent agreement with observed enantioselectivity,[18] the formation of the (*S*,*R*)-product has the lowest activation barrier ($\Delta G^{\ddagger}$) of 66.0 kJ mol^{-1}. It is important to note that the second step in the catalytic cycle of Scheme 4 comprises a series of intermediate processes in which C···C bond formation occurs first and proton transfer follows afterward. The proton transfer step is calculated to have an energy barrier significantly lower than that

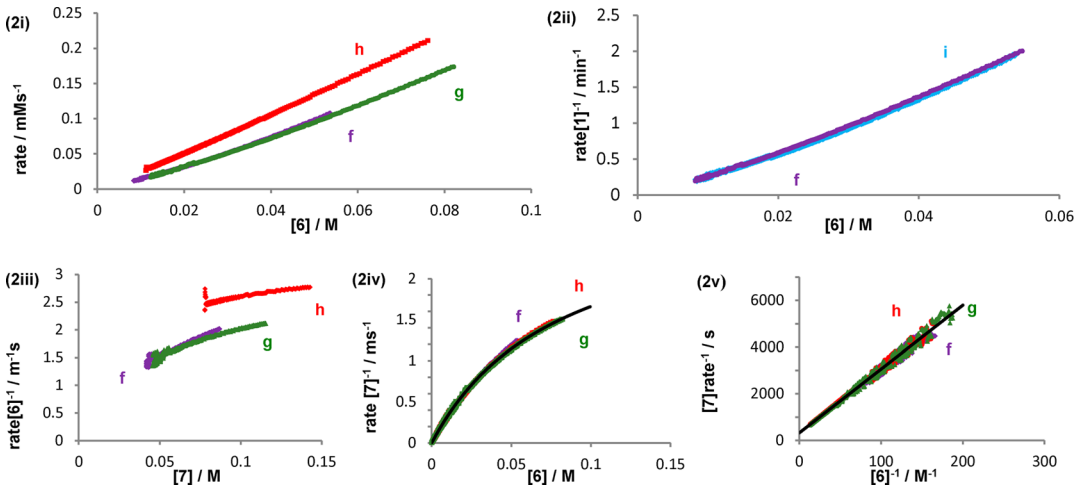

Figure 2. Graphical rate equations for the guanidine-catalyzed addition of a fluorocarbon nucleophile between α-fluoro-β-ketoester and *N*-ethylmaleimide (Scheme 4): (2i) rate vs [**6**], (2ii) rate/[**1**] vs [**6**], (2iii) rate/[**6**] vs [**7**], (2iv) rate/[**7**] vs [**6**], and (2v) [**7**]/rate vs 1/[**6**]. The solid black line represents the kinetic model given in eqs 2 and 3, the Lineweaver–Burk plot of the experimental data, and the solid black line represents the kinetic model given in eq 3. Reaction conditions: (f) $[\mathbf{6}]_0$ = 66.7 mM, $[\mathbf{7}]_0$ = 100 mM, $[\mathbf{1}]_{\text{total}}$ = 3.335 mM; (g) $[\mathbf{6}]_0$ = 100 mM, $[\mathbf{7}]_0$ = 133.3 mM, $[\mathbf{1}]_{\text{total}}$ = 3.335 mM; (h) $[\mathbf{6}]_0$ = 100 mM, $[\mathbf{7}]_0$ = 166.7 mM, $[\mathbf{1}]_{\text{total}}$ = 3.335 mM; (i) $[\mathbf{6}]_0$ = 66.7 mM, $[\mathbf{7}]_0$ = 100 mM, $[\mathbf{1}]_{\text{total}}$ = 6.67 mM.

DOI: 10.1021/acs.joc.5b00709
J. Org. Chem. 2015, 80, 5745–5752

of the C···C bond-forming step (Supporting Information). Therefore, it does not influence the overall reaction rate.

Comparison of Guanidine-Catalyzed Phospha-Michael and Addition Reactions. Both the guanidine-catalyzed phospha-Michael reaction in Scheme 3 and the addition reaction of ketoester **6** to maleimide **7** in Scheme 4 share the same catalytic cycle with two substrates and one catalyst, yet their overall rate expressions are different. This can be rationalized by considering the activation energy barriers in all steps within the catalytic cycle. Using the steady-state approximation, the theoretical expression of the guanidine-catalyzed phospha-Michael reaction is

$$\text{rate} = \frac{\frac{k_1}{k_{-1}}k_2[\mathbf{2}][\mathbf{3}][\mathbf{1}]_{\text{total}}}{1 + \frac{k_1}{k_{-1}}[\mathbf{2}] + \frac{k_2}{k_{-1}}[\mathbf{3}]} \quad (4)$$

By applying the Eyring equation to each rate constant with the calculated relative free energy,[20] we can deduce

$$1 + \frac{k_1}{k_{-1}}[\mathbf{2}] + \frac{k_2}{k_{-1}}[\mathbf{3}] \approx \frac{k_2}{k_{-1}}[\mathbf{3}] \quad (5)$$

The theoretical rate equation (eq 4) can be simplified to rate = $k_1[\mathbf{2}][\mathbf{1}]_{\text{total}}$, which is exactly the empirical rate law of eq 1 derived from the experimental results. Similarly, we computed the entire reaction pathway of the guanidine-catalyzed addition reaction of *α*-fluoro-*β*-ketoester **6** to *N*-ethyl maleimide **7** at the SMD-M06-2X/6-311+G**/M06-2X/6-31G* level (Supporting Information), and the calculated rate constants result in

$$1 + \frac{k_3}{k_{-3}}[\mathbf{6}] + \frac{k_4}{k_{-3}}[\mathbf{7}] \approx 1 + \frac{k_3}{k_{-3}}[\mathbf{6}] \quad (6)$$

The theoretical expression for this reaction can be reduced to

$$\text{rate} = \frac{\frac{k_3}{k_{-3}}k_4[\mathbf{6}][\mathbf{7}][\mathbf{1}]_{\text{total}}}{1 + \frac{k_3}{k_{-3}}[\mathbf{6}]} \quad (7)$$

This rate expression agrees well with the empirical rate law of eq 3 from the experimental results. The relative free energy of activation in each step of the catalytic cycle actually determines the overall rate expression, as well as the overall kinetic behavior. In the guanidine-catalyzed phospha-Michael reaction, the first deprotonation is the rate-determining step. In distinct contrast, the second addition step is the rate-determining step in the guanidine-catalyzed addition reaction of *α*-fluoro-*β*-ketoester **6** to *N*-ethylmaleimide **7**.

Isomerization Reaction of Alk-3-ynoate. Finally, we examine the isomerization reaction of alk-3-ynoate **10** to allenoate **11** catalyzed by guanidine catalyst **1**. It is a 1,3-proton shift reaction and proceeds through two successive hydrogen transfer reactions, namely, deprotonation and protonation (Scheme 5). The first hydrogen transfer step corresponds to the migration of a proton from alk-3-ynoate **10** to guanidine catalyst **1** to form an ion-pair complex **12**. The second step is the transfer of a proton from the guanidinium ion back to the alkynoate with the formation of final isomerized product **11**. This reaction pathway is similar to the monofunctional mechanism proposed by Hu's computational study for the reaction with *tert*-butyl 4-phenybut-3-ynoate instead of *tert*-butyl-5-(phthalimido)pent-3-ynoate, which is used in our kinetic study (Scheme 5).[26]

Scheme 5. Guanidine-Catalyzed Isomerization Reaction of Alk-3-ynoate 10 to Allenoate 11 and Its Monofunctional Mechanism

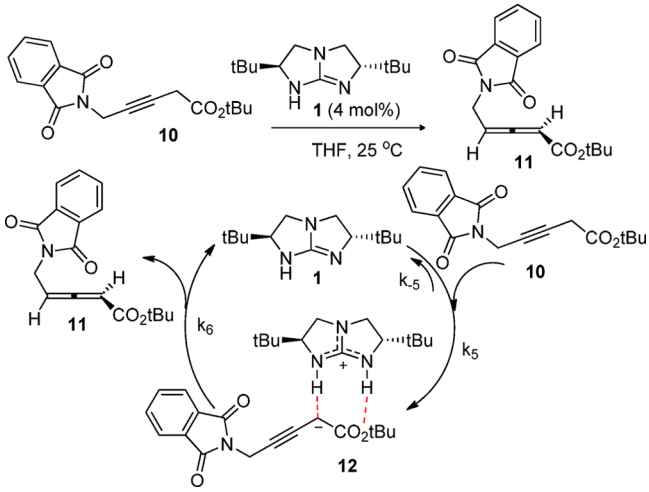

By applying a similar argument as in the case of the guanidine-catalyzed phospha-Michael reaction, we determined the isomerization reaction to be first-order with respect to both alk-3-ynoate ([**10**]) and guanidine ([**1**]) concentration (Figure 3). Hence, the overall rate expression is determined to be

$$\text{rate} = k_5[\mathbf{10}][\mathbf{1}]_{\text{total}} \quad (8)$$

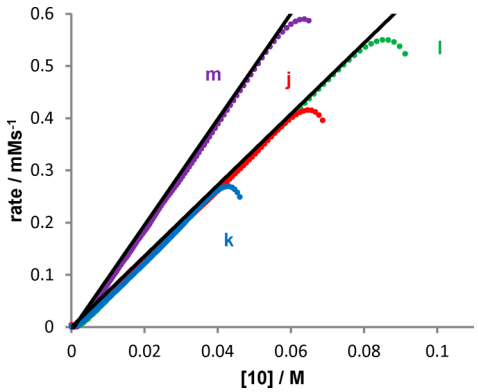

Figure 3. Graphical rate equations for the guanidine-catalyzed isomerization reaction of alk-3-ynoate **10** to allenoate **11** (Scheme 5) (rate vs [**10**]). The solid black lines represent the kinetic model given in eq 8. Reaction conditions: (j) $[\mathbf{10}]_0$ = 75 mM, $[\mathbf{1}]_{\text{total}}$ = 3 mM; (k) $[\mathbf{10}]_0$ = 50 mM, $[\mathbf{1}]_{\text{total}}$ = 3 mM; (l) $[\mathbf{10}]_0$ = 100 mM, $[\mathbf{1}]_{\text{total}}$ = 3 mM; (m) $[\mathbf{10}]_0$ = 75 mM, $[\mathbf{1}]_{\text{total}}$ = 4.5 mM.

where k_5 is determined to be 2.21 M^{-1} s^{-1} (standard deviation of 0.7%; R^2 = 0.997; SSE = 0.0068). This monofunctional mechanism is actually the well-known classical mechanism for enzymatic reaction with reaction rates given by the Michaelis–Menten equation. Its theoretical expression is given by

$$\text{rate} = \frac{k_5k_6[\mathbf{10}][\mathbf{1}]_{\text{total}}}{k_{-5} + k_6 + k_5[\mathbf{10}]} \quad (9)$$

Rate constants k_5, k_{-5}, and k_6 can be computed by using relative free energies from the pathway with the highest turnover frequencies (Supporting Information). Hence, the theoretical rate equation (eq 9) can be reduced to rate = $k_5[\mathbf{10}][\mathbf{5}]_{\text{total}}$ because

DOI: 10.1021/acs.joc.5b00709
J. Org. Chem. 2015, 80, 5745–5752

$$k_{-5} + k_6 + k_5[\mathbf{10}] \approx k_6 \quad (10)$$

This derived rate expression is in good accord with the observed experimental rate equation. The first deprotonation step has an activation energy barrier ($\Delta G^{\ddagger}$ = 84.1 kJ mol^{-1}) higher than that of the second protonation step ($\Delta G^{\ddagger}$ = 14.8 kJ mol^{-1}). Therefore, the first deprotonation step is the rate-determining step, and the overall rate expression is a consequence of this step.

Interestingly, we observed that the reaction is no longer first-order in the concentration of alk-3-ynoate ([**10**]) when its concentration is increased. As evidenced in Figure 4, the

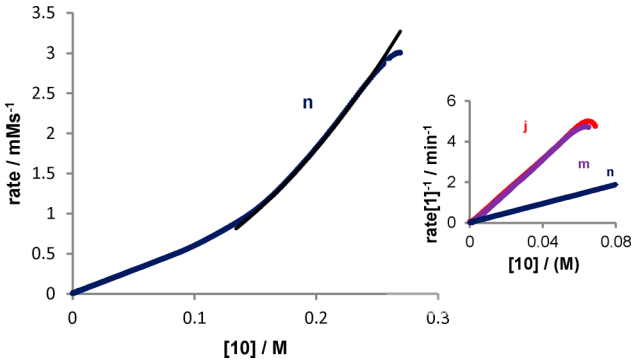

Figure 4. Guanidine-catalyzed isomerization reaction of alk-3-ynoate **10** to allenoate **11** (Scheme 5). The inset shows the rate vs [**10**] and rate/[**1**] vs [**10**]. The solid black curve represents the reaction rate that is linearly proportional to [**10**]^2. Reaction conditions: (n) [**10**]$_0$ = 300 mM, [**1**]$_{total}$ = 15 mM.

reaction rate is determined to be linearly proportional to the square of the concentration of alk-3-ynoate ([**10**]) when the concentration of alk-3-ynoate ([**10**]) is in the range of 0.16–0.24 M. On the basis of this intriguing finding, we propose two possible bifunctional reaction pathways to rationalize this ternary reaction (Scheme 6), namely, bifunctional Brønsted acid activation (pathway A) and bifunctional Brønsted–Lewis acid activation (pathway B).

In both pathways, the first step of hydrogen transfer is the same as in the monofunctional mechanism. However, in the subsequent step, the relatively high concentration of alk-3-ynoate ([**10**]) results in the formation of ternary complex **13** or **14**. In pathway A, the guanidine catalyst forms hydrogen bonds with two molecules of alk-3-ynoate in a side-by-side manner. The alkynoate anion in ternary complex **13** abstracts a hydrogen atom from another molecule of alk-3-ynoate to form product **11**, and ion-pair complex **12** is regenerated simultaneously. For pathway B, because of the electrophilicity of the central carbon in the bicyclic guanidinium ion and the existence of a vacant p orbital on this carbon,[21,25] the oxygen atom of the second alk-3-ynoate can interact with the vacant p orbital of the central carbon in ion-pair complex **12** in a face-on manner to form a different ternary complex **14**. The alkynoate anion in ternary complex **14** could abstract a hydrogen atom from bicyclic guanidinium ion to form product **11**, and at the same time, alk-3-ynoate **10** and guanidine catalyst **1** are regenerated. In this case, the second alk-3-ynoate coordinate to the top face of the guanidinium ion in ternary complex **14** and does not participate in the proton transfer process. Instead, it facilitates the proton transfer process by destabilizing ion-pair complex **12**.

Scheme 6. Proposed Bifunctional Mechanism for the Guanidine-Catalyzed Isomerization Reaction in Scheme 5

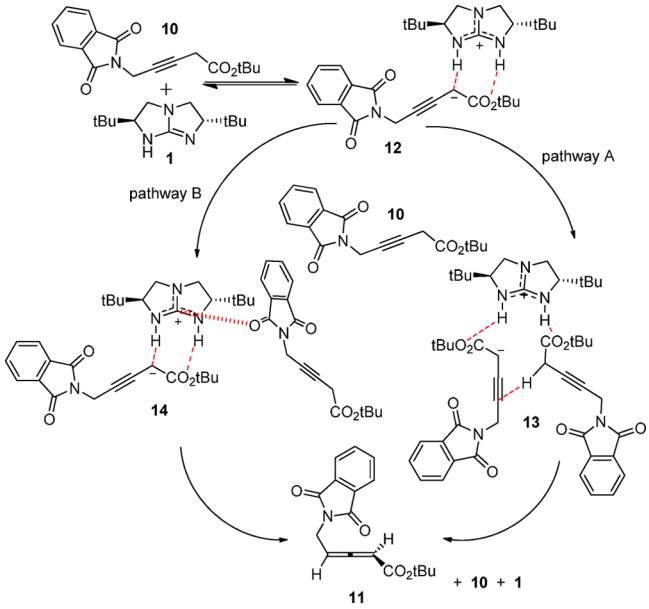

To shed light on the plausible bifunctional mechanism, DFT calculations at the SMD-M06-2X/6-311+G** level were performed for both bifunctional reaction pathways (Supporting Information). The calculated activation barriers ($\Delta G^{\ddagger}$) for the key protonation transfer step leading to the formation of product **11** are 90.0 and 8.3 kJ mol^{-1}, for ternary complexes **13** (via pathway A) and **14** (via pathway B), respectively. When these values are compared with the activation barrier of the second protonation step in the monofunctional mechanism, it is obvious that the bifunctional Brønsted–Lewis acid activation mechanism is favored over the other two pathways. Hence, we envisage that at a higher concentration of alk-3-ynoate ([**10**]), more ternary complex **14** is formed and the proton transfer step from ternary complex **14**, which has an activation barrier lower than that of the monofunctional pathway, yields product **11**. It thus appears that the isomerization reaction follows the monofunctional mechanism at a concentration of alk-3-ynoate ([**10**]) lower than 0.1 M and favors the bifunctional Brønsted–Lewis acid activation mechanism (via pathway B) at higher alk-3-ynoate concentrations. Our proposed monofunctional/bifunctional mechanisms are consistent with observed kinetic behaviors at different substrate concentrations.

From the inset of Figure 4, the overlay of curves j and m in plotting TON versus [**10**] suggests no catalyst deactivation, but the nonoverlay of curve n with curve j or m shows catalyst deactivation. We propose the reaction initiated at a lower alk-3-ynoate concentration with the monofunctional mechanism has no catalyst deactivation. On the contrary, the reaction initiated at a higher alk-3-ynoate concentration with the proposed bifunctional mechanism exhibits catalyst deactivation. Because of the relatively large amount of product formed in reaction n, the oxygen atom of product **11** can interact with the vacant p orbital of the central carbon in ion-pair complex **12** in a face-on manner. As a result, the catalyst loses its activity, and this can account for the results that show there is catalyst deactivation when the reaction initiated at a relatively higher concentration and the catalyst deactivation comes from product inhibition.

DOI: 10.1021/acs.joc.5b00709
J. Org. Chem. 2015, 80, 5745–5752

CONCLUSION

In conclusion, we performed a detailed kinetic study of three different types of chiral bicyclic guanidine-catalyzed reactions, determining the bifunctionality of guanidine catalyst **1**. Although these three reactions share a similar catalytic mechanism, their intrinsic kinetic behaviors are different from each other because of the difference in the rate-determining step in the catalytic cycle. These results also reveal the strong catalytic ability, flexibility, and versatility for the bicyclic guanidine. The theoretical rate expression provides kinetic behavior at a microscopic level, while the experimental kinetic result sheds light on kinetic behavior at a macroscopic level. These two support each other in our study of chiral bicyclic guanidine-catalyzed reactions as we have shown here that the theoretical rate expression for each reaction agrees well with the corresponding experimentally observed rate equation. Our DFT results clarify the catalytic mechanism and readily confirm the experimentally observed kinetic results. This approach should be adopted in the future for kinetic studies of reactions with complicated catalytic mechanisms.

COMPUTATIONAL METHODS

All calculations were performed with the Gaussian 09 programs.[27] DFT calculations were conducted for guanidine-catalyzed addition of α-fluoro-β-ketoester **6** to *N*-ethylmaleimide **7** (Scheme 4) and the guanidine-catalyzed isomerization reaction of alk-3-ynoate **10** to allenoate **11** (Scheme 5). All the equilibrium structures and transition states were fully optimized by using the M06-2X density functional method[28] together with the 6-31G* basis set. The M06-2X functional was chosen in the calculation as it is better suited for handling kinetics, thermodynamics, and noncovalent interactions.[25,28,29] Frequency calculations were performed on the M06-2X/6-31G*-optimized geometries to confirm the nature of the stationary points as they are either equilibrium structures with all the real frequencies or transition states with only one imaginary frequency. Intrinsic reaction coordinate (IRC) calculations were used to confirm the identities of all the transition states. The effect of solvation was evaluated by the SMD implicit solvation model[30] through M06-2X/6-311+G** single-point calculation, based on the gas-phase M06-2X/6-31G*-optimized geometry. Both electrostatic and nonelectrostatic terms are considered in these solvation calculations. The relative Gibbs free energies were computed at M06-2X/6-311+G**//M06-2X/6-31G* level in a toluene solvent (ε = 2.3741) at 298 K for guanidine-catalyzed addition of α-fluoro-β-ketoester **6** to *N*-ethylmaleimide **7** and at the M06-2X/6-311+G**//M06-2X/6-31G* level in a tetrahydrofuran solvent (ε = 7.4257) at 298 K for the guanidine-catalyzed isomerization reaction of alk-3-ynoate **10** to allenoate **11**.

EXPERIMENTAL SECTION

Phospha-Michael Reaction of β-Nitrostyrene. Guanidine **1** (2.23 mg, 0.01 mmol) was dissolved in 1 mL of acetonitrile in the sample vessel containing a stirring bar, and 1 mL of acetonitrile without catalyst was placed inside the reference vessel containing another stirring bar. After the vessels were placed in the calorimeter port while their contents were being stirred, two syringes separately containing 20.2 mg of diphenylphosphine oxide **2** (0.1 mmol) dissolved in 0.8 mL of acetonitrile and 29.8 mg of β-nitrostyrene **3** (0.2 mmol) dissolved in 0.8 mL of acetonitrile were placed in the sample injection port of the calorimeter. Two other syringes separately containing the same amount of diphenylphosphine oxide **2** and β-nitrostyrene **3** in the same amount of solvent were placed in the reference injection port of the calorimeter. A rubber seal was placed at the end of the needles to prevent evaporation of solvent from the syringe. The reaction vessels and these four syringes were allowed to thermally equilibrate (approximately 40−60 min). Once thermal equilibrium was reached, the reaction was initiated by the injection of diphenylphosphine oxide **2** and β-nitrostyrene **3** at the same time into the sample vessel, as well as the reference vessel. The total volume for the reaction is 2.6 mL.

Addition Reaction of Fluorocarbon Nucleophiles. Guanidine **1** (1.12 mg, 0.005 mmol) was dissolved in 0.5 mL of toluene inside the sample vessel containing a stirring bar, and 0.5 mL of toluene without catalyst was placed inside the reference vessel containing a stirring bar. After the vessels were placed in the calorimeter port while the contents were being stirred, two syringes separately containing 21.0 mg of α-fluoro-β-ketoester **6** (0.1 mmol) dissolved in 0.5 mL of toluene and 18.8 mg of *N*-ethylmaleimide **7** (0.15 mmol) dissolved in 0.5 mL of toluene were placed in the sample injection port of the calorimeter. Two other syringes separately containing the same amount of α-fluoro-β-ketoester **6** and *N*-ethylmaleimide **7** in the same amount of solvent were placed in the reference injection port of the calorimeter. A rubber seal was placed at the end of the needles to prevent evaporation of solvent from the syringe. The reaction vessels and these four syringes were allowed to thermally equilibrate (approximately 40−60 min). Once thermal equilibrium was reached, the reaction was initiated by the injection of α-fluoro-β-ketoester **6** and *N*-ethylmaleimide **7** at the same time into the sample vessel, as well as the reference vessel. The total volume for the reaction is 1.5 mL.

Isomerization Reaction of Alk-3-ynoate. The reaction was conducted under N_2 protection. Guanidine **1** (1.38 mg, 0.006 mmol) was dissolved in 0.5 mL of tetrahydrofuran inside the sample vessel containing a stirring bar, and 0.5 mL of tetrahydrofuran without the catalyst was placed inside the reference vessel containing a stirring bar. After the vessels were placed in the calorimeter port while the contents were being stirred, one syringe containing 44.9 mg of alk-3-ynoate **10** (0.15 mmol) dissolved in 1.5 mL of tetrahydrofuran (prepared under N_2 protection) was placed in the sample injection port of the calorimeter and another syringe containing the same amount of alk-3-ynoate **10** in the same amount of solvent (prepared under N_2 protection) was placed in the reference injection port of the calorimeter. A rubber seal was placed at the end of the needles to prevent evaporation of solvent from the syringe. The reaction vessels and the two syringes were allowed to thermally equilibrate (approximately 40−60 min). Once thermal equilibrium was reached, the reaction was initiated by the injection of alk-3-ynoate **10** into the sample vessel, as well as the reference vessel. The total volume for the reaction is 2 mL.

Validation of Calorimetry for Reaction Analysis. The *in situ* calorimetry technique needs to be calibrated with an independent analytical method. Therefore, the final conversion determined from calorimetry was compared to conversion by FTIR measurement to confirm that the observed heat flow represents an accurate measure of the rate of the reaction being studied. Figures 4, 5, and 6 show comparisons of conversion measured by heat flow to the conversion measured by FRIT for the reactions in Schemes 4, 5, and 6, respectively.

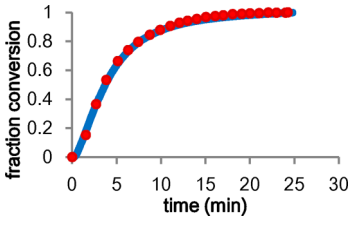

Figure 5. Comparison of conversion measured by heat flow to the conversion measured by FRIT for the reaction in Scheme 3. Reaction conditions: $[\mathbf{2}]_0$ = 57.7 mM, $[\mathbf{3}]_0$ = 96.2 mM, $[\mathbf{1}]_{total}$ = 3.84 mM.

DOI: 10.1021/acs.joc.5b00709
J. Org. Chem. 2015, 80, 5745−5752

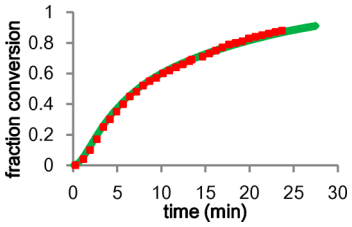

Figure 6. Comparison of conversion measured by heat flow to the conversion measured by FRIT for the reaction in Scheme 4. Reaction conditions: $[\mathbf{6}]_0$ = 66.7 mM, $[\mathbf{7}]_0$ = 100 mM, $[\mathbf{1}]_{total}$ = 3.335 mM.

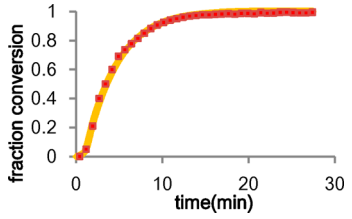

Figure 7. Comparison of conversion measured by heat flow to the conversion measured by FRIT for the reaction in Scheme 5. Reaction conditions: $[\mathbf{10}]_0$ = 75 mM, $[\mathbf{1}]_{total}$ = 3 mM.

■ ASSOCIATED CONTENT

Supporting Information

Kinetic data and computational data. The Supporting Information is available free of charge on the ACS Publications website at DOI: 10.1021/acs.joc.5b00709.

■ AUTHOR INFORMATION

Corresponding Authors

*E-mail: chmwmw@nus.edu.sg.
*E-mail: choonhong@ntu.edu.sg.

Notes

The authors declare no competing financial interest.

■ ACKNOWLEDGMENTS

We gratefully acknowledge the financial support by grants from NTU (M4080946.110, M4081324.110, RG 6/12 M4011018.110, and M4011372.110) and NUS (R-143-000-481-112).

■ REFERENCES

(1) Fu, X.; Tan, C.-H. *Chem. Commun.* **2011**, *47*, 8210−8222.
(2) (a) Dalko, P. I.; Moisan, L. *Angew. Chem.* **2001**, *113*, 3840−3864; *Angew. Chem., Int. Ed.* **2001**, *40*, 3726−3748. (b) Dalko, P. I.; Moisan, L. *Angew. Chem.* **2004**, *43*, 5248−5286; *Angew. Chem., Int. Ed.* **2004**, *116*, 5138−5175.
(3) Doyle, A. G.; Jacobsen, E. N. *Chem. Rev.* **2007**, *107*, 5713−5743.
(4) Alcazar, V.; Moran, J. R.; Demendoza, J. *Tetrahedron Lett.* **1995**, *36*, 3941−3944.
(5) Ma, D. W.; Cheng, K. J. *Tetrahedron: Asymmetry* **1999**, *10*, 713−719.
(6) (a) Takada, K.; Takemura, N.; Cho, K.; Sohtome, Y.; Nagasawa, K. *Tetrahedron Lett.* **2008**, *49*, 1623−1626. (b) Sohtome, Y.; Takemura, N.; Takada, K.; Takagi, R.; Iguchi, T.; Nagasawa, K. *Chem.—Asian J.* **2007**, *2*, 1150−1160. (c) Sohtome, Y.; Hashimoto, Y.; Nagasawa, K. *Eur. J. Org. Chem.* **2006**, 2894−2897. (d) Sohtome, Y.; Hashimoto, Y.; Nagasawa, K. *Adv. Synth. Catal.* **2005**, *347*, 1643−1648. (e) Sohtome, Y.; Takemura, N.; Iguchi, T.; Hashimoto, Y.; Nagasawa, K. *Synlett* **2006**, 144−146.
(7) Shin, B.; Tanaka, S.; Kita, T.; Hashimoto, Y.; Nagasawa, K. *Heterocycles* **2008**, *76*, 801−810.
(8) Uyeda, C.; Jacobsen, E. N. *J. Am. Chem. Soc.* **2008**, *130*, 9228−9229.
(9) (a) Ishikawa, T.; Araki, Y.; Kumamoto, T.; Seki, H.; Fukuda, K.; Isobe, T. *Chem. Commun.* **2001**, 245−246. (b) Ryoda, A.; Yajima, N.; Haga, T.; Kumamoto, T.; Nakanishi, W.; Kawahata, M.; Yamaguchi, K.; Ishikawa, T. *J. Org. Chem.* **2008**, *73*, 133−141. (c) Zhang, G.; Kumamoto, T.; Heima, T.; Ishikawa, T. *Tetrahedron Lett.* **2010**, *51*, 3927−3930.
(10) Saito, N.; Ryoda, A.; Nakanishi, W.; Kumamoto, T.; Ishikawa, T. *Eur. J. Org. Chem.* **2008**, 2759−2766.
(11) Dong, S. X.; Liu, X. H.; Chen, X. H.; Mei, F.; Zhang, Y. L.; Gao, B.; Lin, L. L.; Feng, X. M. *J. Am. Chem. Soc.* **2010**, *132*, 10650−10651.
(12) Zhang, Y.; Kee, C. W.; Lee, R.; Fu, X. A.; Soh, J. Y. T.; Loh, E. M. F.; Huang, K. W.; Tan, C.-H. *Chem. Commun.* **2011**, *47*, 3897−3899.
(13) Corey, E. J.; Grogan, M. J. *Org. Lett.* **1999**, *1*, 157−160.
(14) Peng, B.; Cheng, K. J.; Ma, D. W. *Chin. J. Chem.* **2000**, *18*, 411−413.
(15) Yu, Z. P.; Liu, X. H.; Zhou, L.; Lin, L. L.; Feng, X. M. *Angew. Chem.* **2009**, *121*, 5297−5300; *Angew. Chem., Int. Ed.* **2009**, *48*, 5195−5198.
(16) Ube, H.; Shimada, N.; Terada, M. *Angew. Chem.* **2010**, *122*, 1902−1905; *Angew. Chem., Int. Ed.* **2010**, *49*, 1858−1861.
(17) Lee, R.; Lim, X.; Chen, T.; Tan, G. K.; Tan, C.-H.; Huang, K. W. *Tetrahedron Lett.* **2009**, *50*, 1560−1562.
(18) Jiang, Z. Y.; Pan, Y. H.; Zhao, Y. J.; Ma, T.; Lee, R.; Yang, Y. Y.; Huang, K. W.; Wong, M. W.; Tan, C.-H. *Angew. Chem.* **2009**, *121*, 3681−3685; *Angew. Chem., Int. Ed.* **2009**, *48*, 3627−3631.
(19) Pan, Y. H.; Kee, C. W.; Jiang, Z. Y.; Ma, T.; Zhao, Y. J.; Yang, Y. Y.; Xue, H. S.; Tan, C.-H. *Chem.—Eur. J.* **2011**, *17*, 8363−8370.
(20) Cho, B.; Tan, C.-H.; Wong, M. W. *Org. Biomol. Chem.* **2011**, *9*, 4550−4557.
(21) Cho, B.; Tan, C.-H.; Wong, M. W. *J. Org. Chem.* **2012**, *77*, 6553−6562.
(22) (a) Blackmond, D. G. *Angew. Chem.* **2005**, *117*, 4374−4393; *Angew. Chem., Int. Ed.* **2005**, *44*, 4302−4320. (b) Mathew, J. S.; Klussmann, M.; Iwamura, H.; Valera, F.; Futran, A.; Emanuelsson, E. A. C.; Blackmond, D. G. *J. Org. Chem.* **2006**, *71*, 4711−4722. (c) Rosner, T.; Le Bars, J.; Pfaltz, A.; Blackmond, D. G. *J. Am. Chem. Soc.* **2001**, *123*, 1848−1855. (d) Singh, U. K.; Strieter, E. R.; Blackmond, D. G.; Buchwald, S. L. *J. Am. Chem. Soc.* **2002**, *124*, 14104−14114. (e) Nielsen, L. P. C.; Stevenson, C. P.; Blackmond, D. G.; Jacobsen, E. N. *J. Am. Chem. Soc.* **2004**, *126*, 1360−1362. (f) Mathew, S. P.; Gunathilagan, S.; Roberts, S. M.; Blackmond, D. G. *Org. Lett.* **2005**, *7*, 4847−4850.
(23) Fu, X.; Jiang, Z. Y.; Tan, C.-H. *Chem. Commun.* **2007**, 5058−5060.
(24) Liu, H. J.; Leow, D.; Huang, K. W.; Tan, C.-H. *J. Am. Chem. Soc.* **2009**, *131*, 7212−7213.
(25) Wong, M. W.; Ng, A. M. E. *Aust. J. Chem.* **2014**, *67*, 1100−1109.
(26) Huang, D. F.; Qin, S.; Hu, C. W. *Org. Biomol. Chem.* **2011**, *9*, 6034−6039.
(27) Frisch, M. J.; Trucks, G. W.; Schlegel, H. B.; Scuseria, G. E.; Robb, M. A.; Cheeseman, J. R.; Scalmani, G.; Barone, V.; Mennucci, B.; Petersson, G. A.; Nakatsuji, H.; Caricato, M.; Li, X.; Hratchian, H. P.; Izmaylov, A. F.; Bloino, J.; Zheng, G.; Sonnenberg, J. L.; Hada, M.; Ehara, M.; Toyota, K.; Fukuda, R.; Hasegawa, J.; Ishida, M.; Nakajima, T.; Honda, Y.; Kitao, O.; Nakai, H.; Vreven, T.; Montgomery, J. A., Jr.; Peralta, J. E.; Ogliaro, F.; Bearpark, M.; Heyd, J. J.; Brothers, E.; Kudin, K. N.; Staroverov, V. N.; Kobayashi, R.; Normand, J.; Raghavachari, K.; Rendell, A.; Burant, J. C.; Iyengar, S. S.; Tomasi, J.; Cossi, M.; Rega, N.; Millam, J. M.; Klene, M.; Knox, J. E.; Cross, J. B.; Bakken, V.; Adamo, C.; Jaramillo, J.; Gomperts, R.; Stratmann, R. E.; Yazyev, O.; Austin, A. J.; Cammi, R.; Pomelli, C.; Ochterski, J. W.; Martin, R. L.; Morokuma, K.; Zakrzewski, V. G.; Voth, G. A.; Salvador, P.; Dannenberg, J. J.; Dapprich, S.; Daniels, A. D.; Farkas, Ö.; Foresman, J. B.; Ortiz, J. V.; Cioslowski, J.; Fox, D. J. *Gaussian 09*; Gaussian, Inc.: Wallingford, CT, 2009.

DOI: 10.1021/acs.joc.5b00709
J. Org. Chem. 2015, 80, 5745−5752

(28) (a) Zhao, Y.; Truhlar, D. G. *Acc. Chem. Res.* **2008**, *41*, 157−167. (b) Zhao, Y.; Truhlar, D. G. *Theor. Chem. Acc.* **2008**, *120*, 215−241.
(29) (a) Yang, H.; Wong, M. W. *J. Org. Chem.* **2011**, *76*, 7399−7405. (b) Cho, B.; Tan, C.-H.; Wong, M. W. *J. Org. Chem.* **2012**, *77*, 6553−6562. (c) Yang, H.; Wong, M. W. *J. Am. Chem. Soc.* **2013**, *135*, 5808−5818.
(30) Marenich, A. V.; Cramer, C. J.; Truhlar, D. G. *J. Phys. Chem. B* **2009**, *113*, 6378−6396.

DOI: 10.1021/acs.joc.5b00709
J. Org. Chem. 2015, 80, 5745−5752